CANCER IMAGING

Metastatic status of sentinel lymph nodes in melanoma determined noninvasively with multispectral optoacoustic imaging

Ingo Stoffels,^{1,2,3} Stefan Morscher,^{4,5} Iris Helfrich,^{1,2,3} Uwe Hillen,^{1,2,3} Julia Lehy,^{1,2,3} Neal C. Burton,⁴ Thomas C. P. Sardella,⁴ Jing Claussen,⁴ Thorsten D. Poeppel,⁶ Hagen S. Bachmann,⁷ Alexander Roesch,^{1,2,3} Klaus Griewank,^{1,2,3} Dirk Schadendorf,^{1,2,3} Matthias Gunzer,⁸ Joachim Klode^{1,2,3}*

Sentinel lymph node (SLN) excision is included in various cancer guidelines to identify microscopic metastatic disease. Although effective, SLN excision is an invasive procedure requiring radioactive tracing. Novel imaging approaches assessing SLN metastatic status could improve or replace conventional lymph node excision protocols. In our first-in-human study, we used noninvasive multispectral optoacoustic tomography (MSOT) to image SLNs ex vivo and in vivo in patients with melanoma, to determine metastatic status. MSOT significantly improved the tumor metastasis detection rate in excised SLN (506 SLNs from 214 melanoma patients) compared with the conventional EORTC (European Organisation for Research and Treatment of Cancer) Melanoma Group protocol (22.9% versus 14.2%). MSOT combined with the near-infrared fluorophore indocyanine green reliably visualized SLNs in vivo in 20 patients, up to 5-cm penetration and with 100% concordance with ^{99m}Tc-marked SLN lymphoscintigraphy. MSOT identified cancer-free SLNs in vivo and ex vivo without a single false negative (189 total lymph nodes), with 100% sensitivity and 48 to 62% specificity. Our findings indicate that a noninvasive, nonradioactive MSOT-based approach can identify and determine SLN status and confidently rule out the presence of metastasis. The study further demonstrates that optoacoustic imaging strategies can improve the identification of SLN metastasis as an alternative to current invasive SLN excision protocols.

INTRODUCTION

According to the World Health Organization, the incidence of melanoma is increasing faster than any other major cancer in the world. Melanoma is the fifth most common cancer in the United States, posing a substantial health and economic burden (1). Melanoma metastasizes early into regional lymph nodes (2, 3), requiring sentinel lymph node (SLN) histological status for prognostication and determination of patient survival (4–6). Sentinel lymph node excision (SLNE) is therefore an important diagnostic procedure (7, 8) recommended in the current 2009 American Joint Committee on Cancer (AJCC) guidelines for patients with a primary melanoma (T2, T3, and T4) and clinically uninvolved regional lymph nodes (9).

Widely used for decades, SLNE with histological analysis has proved to be effective and reliable, but it does have drawbacks. The gold standard for targeted extirpation of the SLN is lymphoscintigraphy using 99m-technetium (^{99m}Tc), which invariably represents a radioactive burden for patients and (to a lesser degree) caregivers (*10*). SLNE is further a cost-intensive intervention with potential morbidity, not found to improve overall patient survival (*11*, *12*). Because only a portion of the

¹Department of Dermatology, Venerology, and Allergology, University Hospital Essen, University of Duisburg-Essen, 45122 Essen, Germany. ²West German Cancer Center, University of Duisburg-Essen, 45122 Essen, Germany. ³German Cancer Consortium (DKTK), 69120 Heidelberg, Germany. ⁴Thera Medical GmbH, 81379 München, Germany. ⁵Institute for Biological and Medical Imaging, Technische Universität München, and Helmholtz Center Munich, 85764 München, Germany. ⁶Department of Nuclear Medicine, University of Duisburg-Essen, 45122 Essen, Germany. ⁷Institute of Pharmacogenetics, University Hospital Essen, University of Duisburg-Essen, 45122 Essen, Germany. ⁸Institute for Experimental Immunology and Imaging, Imaging Center Essen (IMCES), University Hospital Essen, University of Duisburg-Essen, 45122 Essen, Germany.

node is sampled for histology, the optimal mode of pathological sectioning remains controversial (13) and could in part explain the high false-negative rate of SLNE reported (9 to 44%) (14). In the Multicenter Selective Lymphadenectomy Trial, 79.2% of melanoma patients who underwent SLNE were histologically negative (15). If a noninvasive approach could reliably exclude metastasis of the SLN, nearly 80% of patients could be spared SLNE surgery (16).

Recently introduced photoacoustic, or multispectral optoacoustic tomography (MSOT) (17, 18), technology allows visualization of fluorescent dyes, such as the near-infrared (NIR) indocyanine green (ICG) or endogenous chromophores like melanin, as contrast agents (19). In animals and resected human tissues, these imaging technologies have been shown to provide additional biologic information on different types of cancer (20–22). Therefore, malignant melanoma, as a melanin-containing tumor, is a suitable candidate to use endogenous chromophores like melanin as the target structure.

MSOT enables operation in real time by capturing single cross-sectional images in <1 ms. The technique illuminates the imaged object with pulsed light at multiple wavelengths and records the ultrasonic signals generated in response to light absorption in a tomographic detection setting (23). Tomographic reconstruction and spectral processing then allow three-dimensional (3D) imaging of tissue chromophores and extrinsic biomarkers with distinct spectral signatures (18, 24). Optoacoustic imaging has previously been used to visualize melanin distribution in B16 skin melanoma tumor-bearing mice (25). Nodal accumulation of melanin in a mouse model of cancer was first demonstrated using a vaccinia virus to drive expression of melanin in cancer cells (26). Small-scale feasibility studies (n < 10) were conducted in dogs (27) and later in humans on explanted SLNs (20, 21), showing an excellent correlation

^{*}Corresponding author. E-mail: joachim.klode@uk-essen.de

between intact photoacoustic melanin detection and histological analysis. However, the utility of this approach relative to the standard of care has not previously been evaluated.

The first goal of our study was to determine whether MSOT-guided pathological evaluation of excised human SLNs would improve the detection of metastasis in comparison with the conventional EORTC (European Organisation for Research and Treatment of Cancer) Melanoma Group protocol. Using the fluorescent dye ICG, we further proceeded to assess in a clinical study the ability of MSOT to identify SLNs and associated metastases in vivo in patients with melanoma. These data were acquired in a cross-sectional study comparing MSOT with standard ^{99m}Tc-guided SLNE and pathological SLN analysis, with the goals of assessing any advantages over the current standard of care and potentially suggesting translation of this noninvasive imaging approach to optimized diagnoses of metastatic cancers.

RESULTS

Ex vivo human melanoma SLN analysis

We analyzed SLNs from 214 patients who underwent SLNE; this cohort is described as the "ex vivo cohort" (table S1). Only patients with a Breslow thickness (BI) of ≥1.0 mm were included (range, 1.0 to 13.0 mm). Patients showed no differences in sex, age, and tumor thickness—the latter a commonly used clinical predictor of metastasis. There was no difference in scope or type of testing. Excised SLNs were imaged by MSOT, providing a color distinction of hemoglobin and melanin (Fig. 1A). Images were acquired in cross section (Fig. 1B) through translation of the SLN in the axial plane; volumetric rendering of the entire image

stack (movie S1) enabled lateral views (Fig. 1A) as well as 3D visualizations (Fig. 1C). Quantification of melanin signal throughout the SLN allowed for a correlation between MSOT output and localization of metastatic cells (Fig. 1, A and D), which was confirmed by histology (Fig. 1E). Knowledge of melanin distribution in the lymph node was used to guide how the SLN was sectioned.

In total, 506 SLN were removed from 214 patients (table S1). Of the 214 patients/506 SLNs in this study, 65 patients (148 SLNs) were assessed by MSOT ex vivo and histology, and 149 patients (358 SLNs) were previously assessed by histology only (28). Four patients with amelanotic melanomas were included in the MSOT cohort. Figure 2A shows a MIP of a lateral view of a patient where histology did not reveal a metastasis (also, no MSOT signal). Suggested sampling positions based on signal intensity for histopathology are marked as dotted lines in the corresponding melanin distribution plot. MSOT+/histology- SLNs were characterized by deposition of melanophages and other sources of pigment, but with no metastasis (MelanA) detected by histology (Fig. 2B). In contrast, MSOT+/histology+ SLN showed high melanin signal by MSOT and histology staining for MelanA was positive (Fig. 2C). There was no false-negative detection via MSOT in this ex vivo evaluation (n = 148).

Metastatic SLN was confirmed by histology in 22.9% of samples in the MSOT cohort and 14.2% of samples in the control cohort. Among the 148 SLNs in the MSOT cohort, a melanin signal (MSOT⁺) was detected in 77 SLNs (52.1%) (Table 1), labeling them as "suspect." Upon follow-up with histology, only 34 of these were determined to be metastatic. In 22 of the remaining 43 MSOT⁺ (but nonmetastatic) cases, histology revealed likely sources of melanin-like spectral signals: 12 capsular nevi, 10 hemorrhage, 5 melanocytic lesions, 6 melanophages,

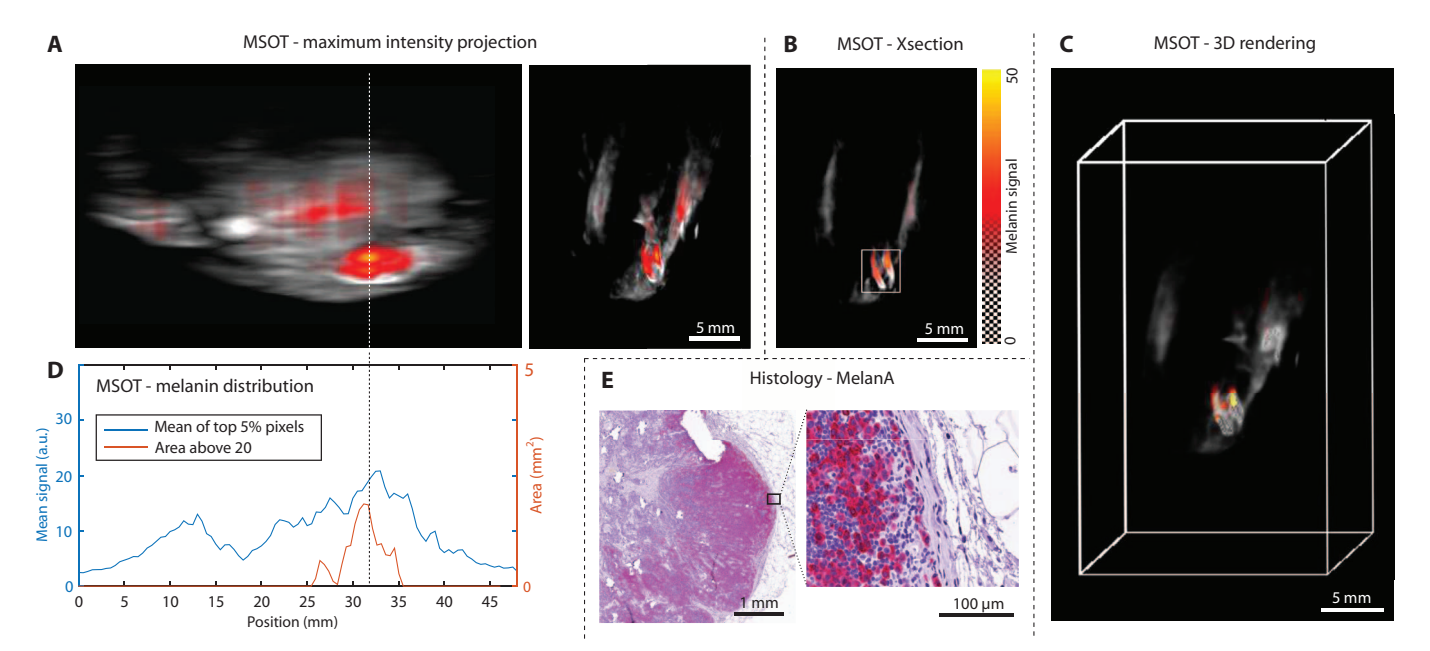


Fig. 1. Ex vivo optoacoustic and histological analysis of a human lymph node from a melanoma patient. (A to E) Grayscale pixels represent the hemoglobin background, whereas the colored overlay shows multispectrally resolved signals specific for melanin. (A) Maximum intensity projections (MIPS) of the lymph node in lateral and axial views, respectively. (D)

Signal distribution along the lateral axis. A single cross section is depicted in (B) [location marked by dashed line in (A) and (D)], with (E) showing the corresponding MelanA stain at low and high magnifications. a.u., arbitrary unit. (C) Three-dimensional rendering of the MSOT image data displayed in (A).

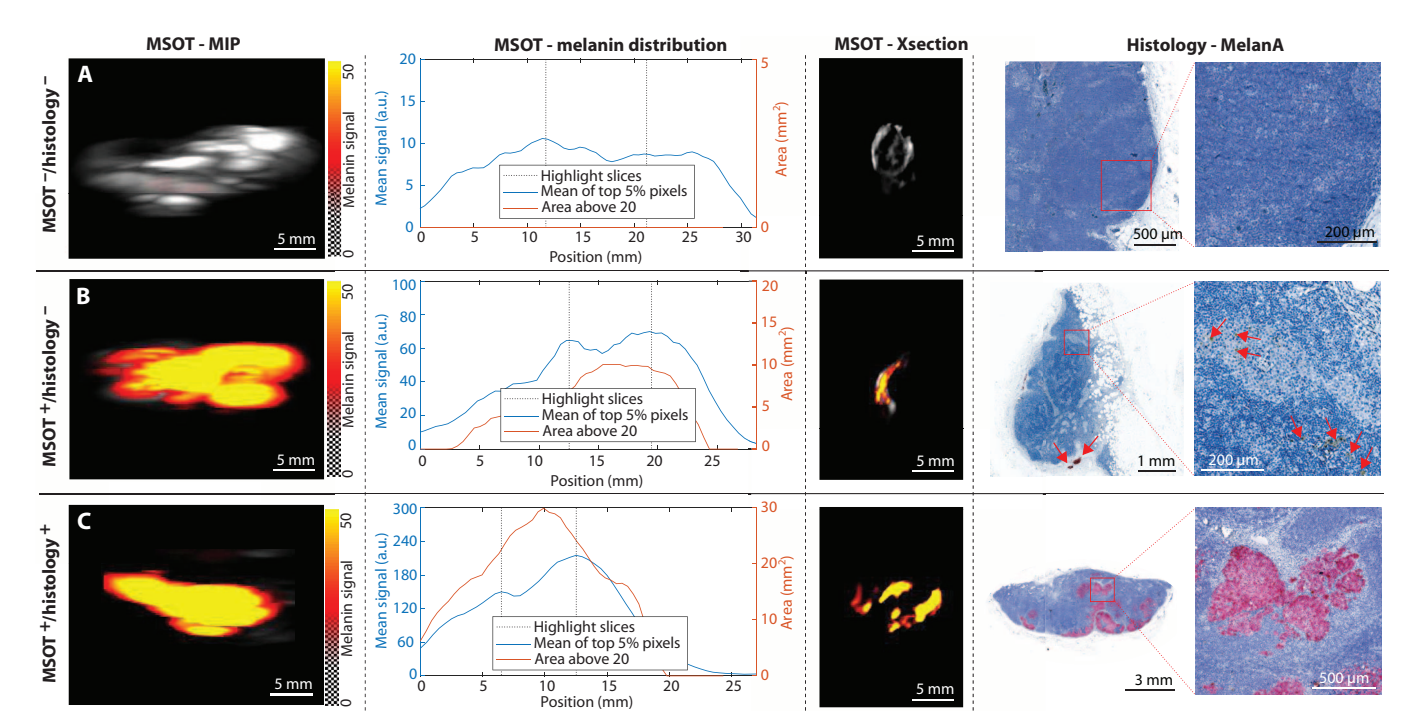


Fig. 2. Comparison of SLN analysis of patients with and without metastasis. (A) MIP of a lateral view of a patient where histology did not reveal a metastasis. The melanin distribution, depicted along the lateral axis, suggested sampling positions based on signal intensity for histopathology marked as dotted lines in the plot. The third column shows an example cross section, with a histological section stained for MelanA at low and high magnifications in the fourth column. (B) MSOT and his-

Table 1. Pathological findings and performance of an MSOT scan ex vivo in the preclinical cohort. MSOT was first used to suggest negative or suspect metastases. Metastasis was then determined on the basis of histology (MelanA staining) of 148 scanned lymph nodes from 65 patients (table S1).

	MSOT $(n = 148 \text{ SLNs})$		
	Negative $(n = 71)$	Suspect $(n = 77)$	
Histology			
Negative $(n = 114)$	71 (47.9%)	43 (29.1%)	
Metastasis ($n = 34$)	0 (0.0%)	34 (22.9%)	
Performance			
Sensitivity	100%		
Specificity	62.3	3%	

and 10 pigmented cells. In all 71 MSOT-negative SLNs, there was no sign of metastasis by histology. The ex vivo analysis of SLNs by MSOT revealed a 100% sensitivity and 62% specificity (Table 1).

Threshold of melanoma cells detectable in phantoms

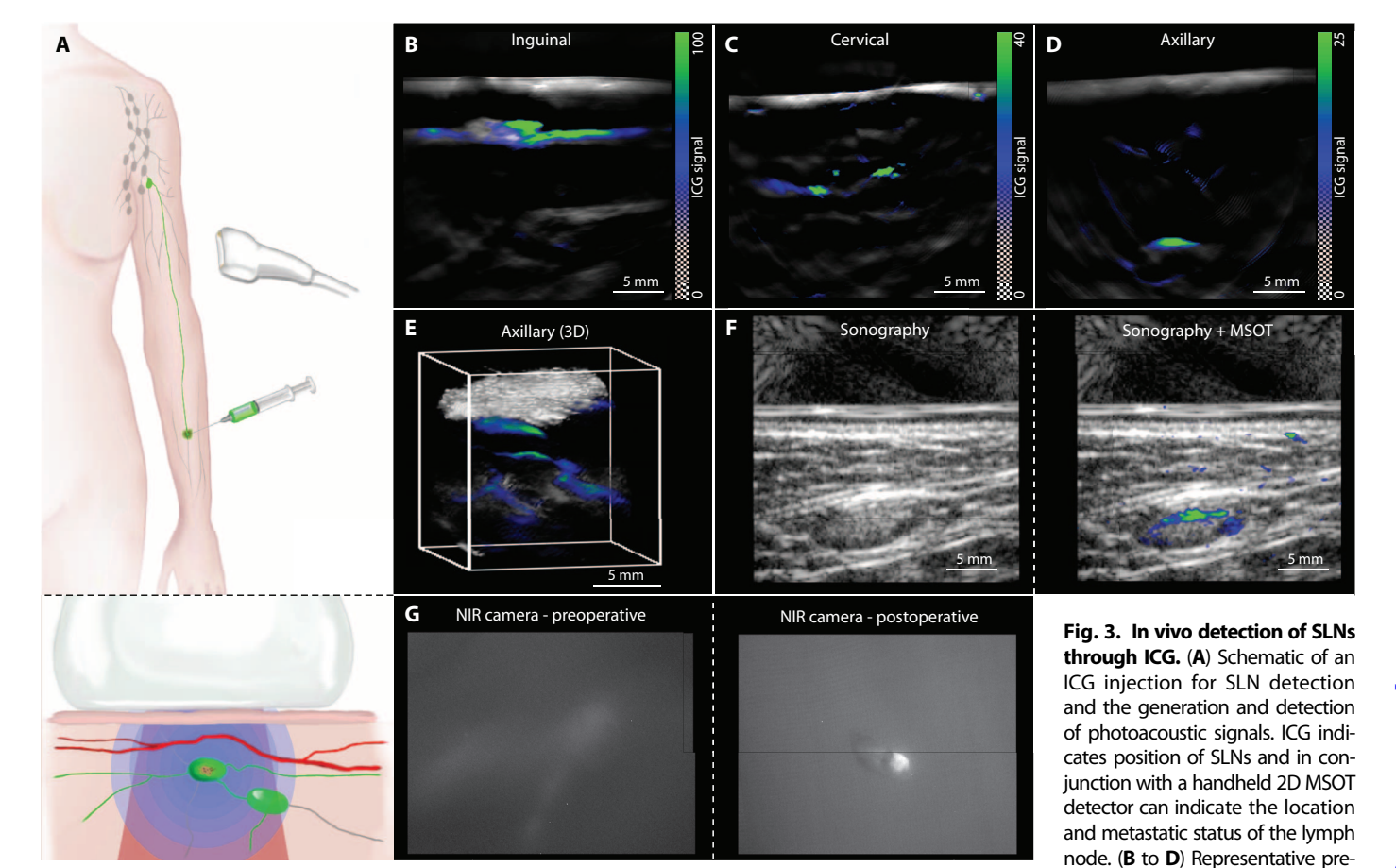
To determine the minimum detectable number of cells with MSOT, we created agarose phantoms with different numbers of murine melanoma cells and imaged and analyzed them using MSOT (fig. S1A). MSOT images were overlaid on corresponding low-magnification light microscopy images to match cell counts to MSOT signal based

tology for a patient with high melanin signal in the MSOT scan, but with no metastasis detected by histology. However, a structure resembling a nevus is marked by red arrows in the low-magnification histology image, whereas individual melanophages are highlighted in the high magnification—both explaining the false-positive signals determined by MSOT analysis. (C) Images of an SLN that was positive for MelanA and was predicted by MSOT.

on spatial orientation (fig. S1B). Individual measurements (n=55) including nonpigmented control cells (n=6) supported a linear relationship between MSOT signal and cell number (not normalized for melanin content) (fig. S1, C and D). MSOT was able to reliably detect as few as four melanoma cells in a volume of 0.02 μ l (fig. S1D). In addition, the linear relationship between melanin concentration (1.5 to 380 μ g/ml) and MSOT signal was shown for a phantom composed of synthetic melanin (fig. S1, E and F).

ICG-based SLN imaging by MSOT in vivo

Twenty patients were enrolled in a trial aiming to detect SLNs by MSOT in vivo (table S2). We administered ICG peritumorally as an exogenous contrast agent with distinct absorption spectra in the NIR and then used a 2D MSOT detector (fig. S2) to image inguinal, cervical, and axillary SLNs (Fig. 3A). In the inguinal SLN example, there was a strong ICG signal in the lymph node, ~5 mm below the skin surface (Fig. 3B). For the cervical SLN, the signal can be seen ~10 mm deep (Fig. 3C). The axillary SLN example localized signal at a depth of ~25 mm (Fig. 3D). Three-dimensional detection with a different MSOT detector provided further volumetric information about the patients' axillary SLNs (Fig. 3E). Pulse-echo ultrasound images of the lymph nodes were taken using the 2D MSOT detector in combination with an experimental integrated ultrasound imaging device that was evaluated to further improve SLN detection. The specific ICG signal simultaneously acquired by MSOT could then be overlaid onto the anatomical reference image based on ultrasound contrast (Fig. 3F). These MSOT results were compared to fluorescence detection of ICG using a



operative images of inguinal, cervical, and axillary SLNs from the 2D detector, with ICG signal overlaid on a single-wavelength background image at 800 nm. Images are from three different patients. (**E**) Rendered view of an SLN imaged using the 3D MSOT detector, showing a network of lymph channels supplying the axillary lymph node of a different patient at ~10 mm. An animated version can be found in movie S3. (**F**) Pulse-echo ultrasound images of a lymph node overlaid with the 2D MSOT image. (**G**) Images of the inguinal SLN [same patient as in (B)] taken by a fluorescence camera before surgery and shortly after the excision.

charge-coupled device (CCD) camera before and after incision of the skin (Fig. 3G). Whereas ICG could not be resolved by fluorescence detection by NRI camera before incision, ICG could be detected at a depth of 50 mm by MSOT noninvasively.

A primary efficacy end point in the trial was the concordance of SLN identified by lymphoscintigraphy and those identified with MSOT by detection of ICG. All lymph node basins identified in lymphoscintigraphy (29 of 29) from the 20 patients were also detected by MSOT. All SLNs visualized by lymphoscintigraphy and single-photon emission computed tomography/computed tomography (SPECT/CT) (n = 41) were also ICG-marked and detected by MSOT, yielding a concordance rate of 100%.

In vivo MSOT imaging of melanin

We compared in vivo imaging results from SLNs that were negative by MSOT and histology (Fig. 4A), positive by MSOT but negative by histology (Fig. 4B), and positive by both MSOT and histology (Fig. 4, C and D). Metastasis and melanin status were evaluated by histology after extirpation (Fig. 4, A to C). As compared to lymphoscintigraphy, which shows the position of the lymph node and primary tumor, MSOT imaging was able to not only localize SLNs via ICG detection but also

provide information regarding metastatic potential in $\mathsf{MSOT}^{^+}$ nodes through melanin detection.

SPECT/CT was used as an additional imaging tool in all patients to determine the depth of the SLN (for instance, 4.03 cm in Fig. 4D). By applying pressure during the MSOT image acquisition, SLNs at greater than 4-cm depth, up to 5 cm, could be detected by reducing the distance between the surface of the skin and the SLN. An entire patient scan with ICG contrast alone or ICG and melanin (movie S2) shows molecular MSOT contrast, in real time, revealing the SLN, afferent lymphatic vessels, and pigment (from a tattoo in this patient) in the SLN.

The in vivo imaging results from all 20 patients were analyzed, and the resulting 41 detected SLNs were classified as positive or negative with respect to melanin content (Table 2). Eighteen SLNs were negative by MSOT and histology (43.9% true negative), 19 were positive by MSOT and negative by histology (46.4% false positive), 4 were positive by both MSOT and histology (9.7% true positive), and no lymph nodes that were negative by MSOT were determined to be positive by histology (0% false negative). This analysis yielded an in vivo sensitivity of 100% and specificity of 48.6%.

After the lymph nodes were extirpated from the in vivo MSOT cohort, the lymph nodes were additionally scanned ex vivo by MSOT

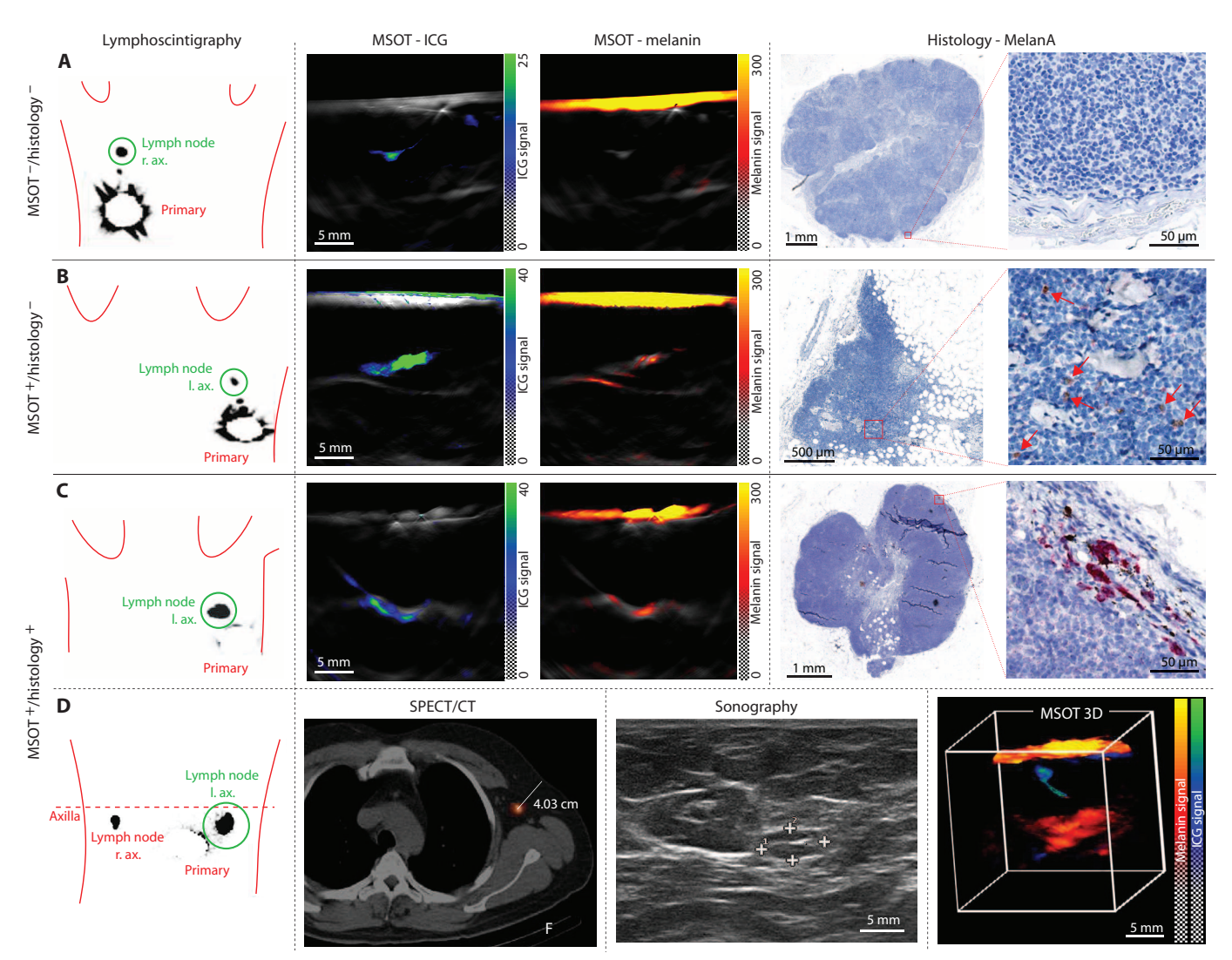


Fig. 4. Preoperative assessment of SLN melanin content using MSOT. In the in vivo clinical cohort (n=20), patients were first imaged by a gamma camera (99m Tc lymphoscintigraphy) to localize the SLNs (left column). MSOT (ICG and melanin), histology, SPECT/CT, and ultrasound were applied to other patients, as indicated for four different patients here. (**A**) Patient with no detectable metastasis. r. ax., right axillary node. (**B**) Patient with a melanin signal in MSOT that is confirmed by the presence of pigmented

cells in the high-magnification histology (marked by red arrows), where no evidence for metastasis was found in histology. I. ax., left axillary node. (**C**) Patient with an SLN that is both MSOT⁺ and positive for staining by MelanA immunohistochemistry. (**D**) SLN with metastasis, per MSOT, alongside SPECT/CT and ultrasound images of the SLN. A combined 3D rendering of an MSOT image taken by the 3D detector shows both melanin and ICG localization in the SLN. A rotating view is in movie S4.

before histological analysis. Among these same 41 SLNs, 26 (63.4%) were MSOT⁺; of these, only 4 were confirmed metastatic by histology (Table 3), giving a sensitivity of 100% and a specificity of 40.5% for the ex vivo analysis. In the remaining 22 MSOT⁺/histology⁻ SLNs, the histology reported spectral absorbers, such as hemorrhage, pigmented cells, tattoo pigment, nevi, or melanophages, which would explain the false-positive MSOT signal. In 15 of the 41 SLNs (36.6%), no melanin signal was detected by MSOT. All of these SLNs were histopathologically negative, indicating no false-negative detection by MSOT (Table 3).

DISCUSSION

In this clinical study, we provide compelling first-in-human evidence that a noninvasive, nonradioactive optoacoustic imaging technology, called MSOT, can complement and enhance existing means of identifying metastatic lymph nodes in melanoma, and possibly other cancers. We demonstrated the utility of MSOT in melanoma patients by using the contrast agent ICG to detect SLN in vivo and by detecting metastases in excised SLNs as a stand-alone imaging approach to guide histological assessment. Although the feasibility of ICG-mediated detection of the SLN via MSOT has been previously demonstrated in animals (27), our study translates these findings to humans, showing the full potential of ICG-MSOT imaging as a nonradioactive alternative to locate the SLN in a patient setting (19).

MSOT SLN detection with ICG was comparable to standard ^{99m}Tc-nanocolloid-guided SLN detection in all possible anatomic regions. Compared with the depth limitations of ICG or fluorescently labeled antibody detection by infrared cameras (16, 29), MSOT can pick up

Table 2. Pathological findings and performance of an MSOT scan in vivo in the clinical cohort. MSOT findings were compared against histology (MelanA staining) to determine the sensitivity and specificity of the imaging technology in identifying metastases in 41 SLNs from n = 20 patients.

	MSOT (n = 41 SLNs)	
Histology	Negative (n = 18)	Suspect $(n = 23)$
Negative ($n = 37$ SLNs)	18 (43.9%)	19 (46.4%)
Metastasis ($n = 4$ SLNs)	0 (0%)	4 (9.7%)
Performance		
Sensitivity	100%	
Specificity	48.6%	

Table 3. Pathological findings and performance of ex vivo MSOT imaging of extirpated SLN from the clinical cohort. In the clinical cohort of 20 patients, SLNs were imaged in vivo and compared with histology (Table 2). The SLNs were then excised and examined again ex vivo by MSOT, and again compared with histology, as reported here.

	Clinical MSOT cohort, ex vivo $(n = 41 \text{ SLNs})$	
	Negative (n = 15)	Suspect $(n = 26)$
Pathological findings, metastasis		
Negative $(n = 37)$	15 (36.6%)	22 (53.7%)
Metastasis $(n = 4)$	0 (0%)	4 (9.7%)
Performance		
Sensitivity	100%	
Specificity	40.5%	

Additional pathological findings in histologically negative SLN with suspect signal in MSOT (n = 22)

Hemorrhage	9 (42.8%)
Pigmented cells	6 (28.6%)
Tattoo pigment	3 (14.2%)
Nevus	2 (9.5%)
Melanocytic lesion	1 (4.7%)
Melanophages	1 (4.7%)

ICG-marked SLNs at a depth determined by SPECT/CT to be up to 5 cm. Similar to another report on rat lymph nodes (19), we demonstrate the possibility of enhanced SLN detection by an integrated optoacoustic/ultrasound system. By combining optoacoustic sensitivity with ultrasound, we were able to obtain in one step the lymph node molecular characteristic and morphology—a process that currently takes two steps in the clinic with preoperative ultrasound followed by radioactive marking of the SLN. These results suggest that MSOT and ultrasound imaging techniques could be a valuable alternative to lymphoscintigraphy, not only in melanoma but also in other malignancies such as breast or squamous cell carcinoma (29). The technique potentially could be further refined to enable opto-

acoustically guided, minimally invasive fine-needle aspiration biopsies of SLNs (30).

Our study evaluated the clinical potential of MSOT for melanoma patients ex vivo and in vivo. Optoacoustic imaging in excised SLNs led to an improved detection rate of metastases in comparison to the EORTC Melanoma Group protocol (22.9% versus 14.2%). This promising result could mean that MSOT-guided histology may be the answer to the long-standing debate of how to correctly section SLNs for histopathological analysis (13, 31–33). We obtained zero false negatives in vivo in 20 patients and ex vivo in the same SLNs from 85 patients. Thus, considering that melanoma metastases are mostly pigmented, excluding the presence of melanin in draining SLNs could represent a new means of noninvasively predicting cancer-free SLNs. Unfortunately, MSOT had a high false-positive rate, likely owing to the presence of other absorbers common to the human system, such as tattoo pigment, capsular nevus, melanophages, or hemorrhage. This also explains the difference between the results of the in vivo and ex vivo measurements of the same SLNs.

The considerable number of cases where melanin signals were noted, but no metastasis was identified (>60% of positives), indicates that SLN excision and histological evaluation will remain essential in $MSOT^+$ cases to rule out cancer (as in the norm currently for lymphoscintigraphy). Alternatively, in cases where no melanin signal is detected, patients would not need to undergo SLN excision, eliminating the need for surgery and the risks, costs, and morbidities associated with it (34). In addition, the use of other optical contrast agents that target melanoma cells (28) could potentially enable a reduction in the false-positive rate observed here by allowing the simultaneous in vivo evaluation of multiple markers of melanoma.

Although not performed in our current study, an advantage of the noninvasive and nonradioactive MSOT imaging approach is that it could be performed repeatedly, allowing SLN to be assessed at various intervals for the appearance of metastasis. The site of the SLN could be documented, and patients could be regularly screened by MSOT to determine whether the melanin content has increased and, in conjunction with conventional ultrasound criteria, an assessment of the likelihood of lymph node metastasis could be made. This method would not need to be restricted to SLNs but could apply to the entire downstream lymph node region and be used as a regular follow-up examination in melanoma patients with higher-stage melanoma disease, such as ≥IIC.

Because MSOT detection of SLN metastasis relies on melanin, a potential caveat of the method could be detecting metastatic deposits of amelanotic melanomas. Four patients with amelanotic melanomas were included in our study; however, none of these were SLN-positive. A previous study that analyzed 75 melanomas determined amelanotic clinically and by routine microscopy demonstrated that at least some melanin was detected in all cases (35), suggesting that lymph node metastasis of amelanotic melanomas may contain enough melanin (36) to be detected by MSOT (movie S3). Future studies will be needed to assess the validity of MSOT analysis in amelanotic melanomas. Another limitation of this study is the temporal separation of the two cohorts in the preclinical setting. This does not, however, affect timeindependent variables such as the metastasis-free SLN detection rate. Although the clinical in vivo study results are promising, they will need to be confirmed in larger patient cohorts, in a multicenter randomized prospective trial.

We believe that the results of our study demonstrate how patients could benefit from incorporating MSOT imaging into the clinical management of melanoma. ICG labeling and MSOT imaging proved to be an excellent approach for SLN detection, eliminating the need for radioactive tracers. MSOT imaging of excised SLNs further was able to improve pathological analysis, increasing metastasis detection rates. The most exciting prospect of this study is the potential of MSOT to be used in vivo to assess SLN status and exclude the presence of metastasis. If validated in larger studies, this approach could alleviate the need for invasive SLNE surgery in a significant number of patients.

MATERIALS AND METHODS

Study design

The objective of this prospective study was to investigate to what extent the optoacoustic technique, in combination with ICG injection, provides a noninvasive and nonradioactive method for the accurate detection and simultaneous diagnosis of SLN status in melanoma patients. The primary end point was the concordance of SLNs identified by lymphoscintigraphy and those identified with MSOT and ICG. Secondary end points of this study were defined as rate of positive SLNs and the false-negative rate. Moreover, the applicability and the possibility of intraoperative detection are to be evaluated in vivo by means of MSOT. For this purpose, the data of the preoperative in vivo MSOT diagnostics should be compared with the findings of post-operative ex vivo diagnostics using MSOT and subsequent histology. Sensitivity was calculated as [true-positive/(true-positive + false-positive)]; specificity was calculated as [true-negative/(true-negative + false-positive)].

To estimate the number of SLNs that needed to be examined, we assumed a detection rate (A + C)/N of 100% for the gold standard ^{99m}Tc method, a discordance rate (B + C)/N of 8%, and set δ at 5%. We found that 93 SLNs (about 37 patients, 2.5 SLNs per patient) needed to be examined to demonstrate equivalence between the two methods with 80% power and type I error (α) of 5%. Therefore, it was our aim to include 20 patients in this cross-sectional trial. In the analysis, results were classified as "concordant" in cases where all patients' SLNs were detected by both methods. The interim analysis of the first 20 patients showed that all SLNs (n = 41) visualized by lymphoscintigraphy and SPECT/CT had also been ICG-labeled and detected by MSOT (n = 41), resulting in a concordance rate of 100%. A further interim analysis examined the assessment of the SLN status regarding metastatic infiltration. The clarity of this result was unexpected and, thus, not considered a major focus in our initial study plan. The results of our initial cross-sectional trial are presented here as a feasibility study.

Sentinel node scintigraphic technique and SPECT/CT

Lymphoscintigraphy and SPECT/CT were performed as previously described (37). Eighty megabecquerels of 99m Tc-nanocolloid was injected around the tumor in four intradermal deposits of 0.1 ml. Dynamic images of the corresponding anatomical region were acquired at 30 s per frame for 5 min with a total of 10 frames. Subsequently, anterior, lateral, and oblique projections were acquired for 5 min each using a dual-detector γ camera with a mounted two-row multidetector CT scanner (Symbia T, Siemens Healthcare). SPECT/CT images of the region in which an SLN was visualized were obtained immediately after the planar images showing an SLN. The reconstructed data were displayed as sagittal, coronal, and axial slices. Inherent image fusions were generated from the co-registered SPECT and low-dose CT images using the e.soft 2007 application package (Siemens Healthcare).

Sentinel lymph node excision

SLNE is performed as a standard procedure at the Department of Dermatology, University Hospital Essen, Germany, according to the guidelines of the Deutsche Dermatologische Gesellschaft (DDG, German Association of Dermatology) (38). The procedure was applied in melanoma patients in AJCC stages I and II (tumor depth of \geq 1.0 mm).

Subsequent SLNE was performed either under tumescent local anesthesia or general anesthesia (39, 40). Preparation and subsequent excision of all marked lymph nodes were carried out via an incision over the location measuring maximum radio-isotype activity by a mobile manual scintillation measuring probe (C-Trak, Care Wise Medical Products Corporation) in the control cohort or by preoperative marking on the skin according to information obtained from SPECT/CT. Surgery was terminated when no further radioactive foci could be traced in the surgical field. The surgical technique was identical in both cohorts. Dyes such as patent blue were not used because of potential allergic reactions and the risk of a permanent tattoo (41).

Patient characteristics of ex vivo cohort

SLNs were obtained from 65 melanoma patients treated in the Department of Dermatology, University Hospital Essen, Germany. The study was approved by the Institutional Review Board of the University of Duisburg-Essen (Ethikkommission der Universität Duisburg-Essen) under the Institutional Review Board protocol no. 12-4961-BO. All patients provided written informed consent.

Two hundred fourteen clinically lymph node–negative patients qualified for subsequent analysis. A patient was defined as clinically lymph node–negative if neither in clinical examination nor in preoperative ultrasound a metastasis could be detected (9). As a reference, we compared the MSOT cohort (n = 65 patients) with a control cohort of SLNE patients (n = 149) analyzed previously (37). The two study cohorts showed no differences in sex, age, ulceration rate, or tumor thickness. Ex vivo cohort characteristics are summarized in table S1.

MSOT imaging of ex vivo SLNs

The commercially available optoacoustic imaging setup used for scanning phantoms and excised SLNs was an MSOT inVision 128 (iThera Medical GmbH). Briefly, samples being imaged were exposed to nanosecond laser pulses generated by an Nd:yttrium-aluminum-garnet (Nd:YAG) pumped optical parametric oscillator (OPO) tunable in 1-nm steps from 680 to 980 nm. For multispectral imaging, 10 equidistant wavelengths between 700 and 880 nm were selected to allow separation of chromophores. Signals were detected using an arc-shaped transducer array with 128 detector elements (center frequency, 5 MHz; transmit/receive bandwidth, 60%) covering 270° around the sample (fig. S3). To optimize the signal-to-noise ratio (SNR), data from 25 laser pulses at a repetition rate of 10 Hz were averaged. Reconstruction of cross-sectional slices with a square field of view of 5×5 cm² using the standard back-projection algorithm (42) was performed after band-pass filtering and deconvolution with the electrical impulse response of the transducer.

The dissected tissue containing the SLNs was placed in paraformaldehyde solution. After 24 hours, the SLNs were separated from surrounding adipose tissue. The SLNs were then mounted in the imaging chamber of the MSOT inVision 128 using a dedicated holder and protected by a thin membrane to avoid contact with water in the imaging chamber. The sample was translated perpendicular to the imaging plane with a motorized stage, and cross-sectional images were

acquired in 0.5-mm intervals along the axis of the lymph node to acquire a 3D volume. The reconstructed images were then used for multispectral post-processing using an unmixing matrix determined by independent component analysis (ICA) using spectral priors (43). ICA was supplied with a confirmed melanin-positive data set and the expected NIR absorption spectrum of melanin to train the spectral unmixing of absorbers, where the result was saved and reapplied to all other data sets to create comparable results in the detection of melanin (43). Composite images displayed here feature a background image acquired at 800 nm, giving anatomical and boundary information for the lymph node, with a pseudocolor overlay using α transparency to depict melanin distribution within the sample.

MATLAB was used to visualize the multispectrally resolved signal specific for melanin as a function of position along the scanned axis of the lymph node to indicate the distribution of melanin throughout the lymph node. SLN melanin signal was deemed suspicious based on intensity, localization, punctuation, and the relationship to background signals. If two independent investigators reported a suspicious melanin signal in the same visual image assessment, then this information was used to suggest two cross sections based on maximum melanin signal and minimum 5.0-mm spacing between them for histological evaluation of the node.

SLN histology in the ex vivo cohort

After the MSOT scan, the dissected SLNs were processed for histological assessment by the pathology department. If melanin was detected by MSOT, the SLNs were lamellated according to the melanin location suggested by MSOT (Fig. 1C). The lamella with the region of interest of the SLN was embedded in a marked capsule and examined according to the protocol in slices every 200 µm. Staining was performed with 1× hematoxylin and eosin (H&E) and 2× with antibodies to S100 and "human melanoma black 45" (HMB 45) for melanoma (44, 45). The rest of the SLN was examined according to the standard protocol lamellated into parallel slices 3 mm thick and paraffin-embedded. Subsequent serial sections were made. Conventional staining was performed with H&E staining as well as immunohistological staining with antibodies to S100, MelanA, and HMB 45. Frozen slide analysis was not performed. All slides were examined by an experienced dermatopathologist. Unusual findings were examined by at least two pathologists, and a consensus diagnosis was reached.

The pathologic workup of the SLNs (control cohort) was performed according to the EORTC Melanoma Group pathology protocol (31). Lymph nodes were bivalved and paraffin-embedded. Three slices were cut for H&E and immunohistochemistry staining (MelanA and protein S100) at a regular 50-µm interval at least six times after the SLN protocol. No polymerase chain reaction analysis was performed.

Patient characteristics of the in vivo cohort

This cross-sectional clinical trial was approved by the Institutional Review Board at the University Hospital Essen (13-5468-BO) and registered at the German Clinical Trials Register (DRKS00005447). All patients had given written consent to be entered into the trial.

Twenty patients, fulfilling the inclusion criteria, with stage Ib or II (AJCC 2009) malignant melanoma and an age >18 years, who were scheduled to undergo SLNE were included in this cross-sectional trial in August 2014. All patients received both ^{99m}Tc-nanocolloid and ICG. Exclusion criteria included age <18 years, pregnancy, lactation, and allergy to iodine or known intolerance to ICG. All patients had given

written informed consent to proceed with both lymphoscintigraphy and MSOT imaging using ICG. Clinical cohort characteristics are summarized in table S2. Both cohorts were treated with the same surgical procedure according to the guidelines of the DDG (38).

Indocyanine green

Shortly before MSOT imaging, a vial of 25-mg ICG (Pulsion Medical Systems AG) was dissolved in 50 ml of water for injection (B. Braun Medical), yielding a concentration of 0.5 mg/ml. One milliliter of dissolved ICG was injected peritumorally 30 min before MSOT imaging.

In vivo MSOT imaging

For in vivo imaging, a prototype MSOT system optimized for handheld operation was used. Nanosecond excitation laser pulses were generated using an OPO pumped by a Nd:YAG laser (Innolas GmbH) at a repetition rate of 20 Hz and a wavelength tuning range from 680 to 980 nm. Two individual detector designs were evaluated in the study. A cylindrically focused 256-element detector array (center frequency, 4 MHz; send/receive bandwidth, 52%; resolution, ~190 μm) and 135° coverage provided 2D cross-sectional images with a field of view of $25 \times 25 \text{ mm}^2$ and a pixel size of 62.5 µm (fig. S3). A second, volumetric detector with 384 detector elements (center frequency, 2.5 MHz; bandwidth, 60%; resolution, ~300 μm) arranged on a semisphere with 110° angular coverage provided a 3D field of view of $20 \times 20 \times 25 \text{ mm}^3$ at equivalent pixel size (fig. S3). Laser light was delivered via a custom-made fiber bundle (CeramOptec GmbH), from next to the detector for 2D imaging and through an aperture in the center of the detector for 3D imaging. Reconstruction using the standard back-projection algorithm (42) was performed after band-pass filtering and deconvolution with the electrical impulse response of the transducer. For multispectral imaging, five wavelengths (700, 730, 760, 800, and 850 nm) were acquired with one pulse per wavelength, and chromophores were unmixed using spectral fitting (43), again visualized as a composite image to combine specific chromophore signal and anatomical background (single-wavelength image of tissue optical absorbance at 800 nm) with full rate in live view. To increase SNR, three subsequent multispectral acquisitions were averaged in post-processing, producing an effective frame rate of 0.75 images/s. Exponential depth correction ($\mu_{eff} = 0.25 \text{ cm}^{-1}$) was applied to approximate depth decay of excitation light and help visualize deep structures. For the 3D detector, the signal outside the approximately spherical field of view was cropped to avoid reconstruction artifacts from insufficient tomographic information in the peripheral areas. Live image display for 3D was visualized through MIPs in three orthogonal planes, whereas images displayed in this work were rendered through the Shear-Warp algorithm in MATLAB in post-processing. If in the visual image assessment, performed by two independent investigators, a suspicious melanin signal was present, the SLN was defined as suspect.

Hybrid ultrasound/MSOT imaging

For a subset of patients, the described 2D handheld detector (fig. S3) was also used to generate a pulse-echo ultrasound image using an experimental ultrasound imaging subsystem. Transmit pulses were sent with a peak-to-peak voltage of 40 V at 6 MHz and reconstructed using synthetic transmit aperture technique (46) at a field of view of 40 \times 40 $\,\mathrm{mm}^2$ with a line density of 6.7 lines/mm. The synthetic transmit aperture method was applied across subapertures of 128 elements each (one-half of the full aperture), with a single element sequentially transmitting the pulse and all elements receiving the resulting echo signals.

Data collected by two subapertures, covering the full-view angle of the handheld array, were then combined into a final single image using spatial compounding technique. After the acquisition of MSOT images, the detector was kept in place on the patient and was replugged into the ultrasound system to allow acquisition of a corresponding ultrasound image. Because of small motions of the detector and patient during that process, the presented overlaid image had to be manually aligned for a match to illustrate the potential of a future, completely integrated combined ultrasound and MSOT imaging system (Fig. 3, F and G).

NIR fluorescence imaging

NIR imaging was performed by the Fluobeam system (Fluoptics). This handheld device is based on a camera and an integrated NIR light source intended to image fluorescent moiety having a maximum absorption between 750 and 800 nm and a maximum emission between 780 and 850 nm. The excitation was provided by a class 1 expanded laser source at 780 nm. The irradiance on the imaging field was 7 mW/cm². The fluorescence signal was collected by a CCD through a high-pass filter with a high transmittance for wavelength >800 nm (Fig. 3, I and J).

Statistical analysis

Differences in patients' characteristics were evaluated with the Wilcoxon-Mann-Whitney test for continuous variables, and the χ^2 test or the Fisher's exact test, the latter when expected cell frequencies were low, for categorical variables. Differences were regarded significant at P < 0.05. For the phantom study, samples with sufficient populations were analyzed by a one-way analysis of variance (ANOVA) with Fisher's least significant difference post hoc test to determine the minimum number of detectable B16-F10 cells that were statistically significantly different from the background level determined from the nonpigmented HCT116 control cells. The statistical analysis was performed with SPSS version 20 (Statistical Package for Social Science, SPSS Inc.).

SUPPLEMENTARY MATERIALS

 $www.science translational medicine.org/cgi/content/full/7/317/317 ra 199/DC1 \\ Methods$

- Fig. S1. Detection limit and signal linearity of MSOT inVision imaging system in phantoms.
- Fig. S2. Characteristics of the ultrasound detectors, as specified by the manufacturer.
- Fig. S3. Multispectral image composition.
- Table S1. Characteristics of 214 melanoma patients in the preclinical ex vivo cohort.
- Table S2. Patient characteristics of the clinical in vivo cohort.
- Movie S1. Flythrough ex vivo lymph node.
- Movie S2. In vivo image sequence of lymph vessels and lymph node.
- Movie S3. Rotating 3D rendering of an ICG-containing lymph node. $\label{eq:containing} % \begin{subarray}{ll} \end{subarray} \begin{suba$
- Movie S4. Sequence of cross-sectional images obtained from an excised lymph node with a hypopigmented melanoma metastasis.

REFERENCES AND NOTES

- E. Livingstone, C. Windemuth-Kieselbach, T. K. Eigentler, R. Rompel, U. Trefzer, D. Nashan,
 S. Rotterdam, S. Ugurel, D. Schadendorf, A first prospective population-based analysis investigating the actual practice of melanoma diagnosis, treatment and follow-up. *Eur. J. Cancer* 47, 1977–1989 (2011).
- C. M. Balch, Surgical management of regional lymph nodes in cutaneous melanoma. J. Am. Acad. Dermatol. 3, 511–524 (1980).
- J. E. Gershenwald, M. I. Ross, Sentinel-lymph-node biopsy for cutaneous melanoma. N. Engl. J. Med. 364. 1738–1745 (2011).
- D. L. Morton, J. F. Thompson, A. J. Cochran, N. Mozzillo, R. Elashoff, R. Essner, O. E. Nieweg,
 D. F. Roses, H. J. Hoekstra, C. P. Karakousis, D. S. Reintgen, B. J. Coventry, E. C. Glass, H.-J. Wang;

- MSLT Group, Sentinel-node biopsy or nodal observation in melanoma. N. Engl. J. Med. 355, 1307–1317 (2006)
- J. E. Gershenwald, W. Thompson, P. F. Mansfield, J. E. Lee, M. I. Colome, C.-h. Tseng, J. J. Lee,
 C. M. Balch, D. S. Reintgen, M. I. Ross, Multi-institutional melanoma lymphatic mapping experience: The prognostic value of sentinel lymph node status in 612 stage I or II melanoma patients. J. Clin. Oncol. 17, 976–983 (1999).
- C. M. Baich, S.-J. Soong, J. E. Gershenwald, J. F. Thompson, D. S. Reintgen, N. Cascinelli, M. Urist, K. M. McMasters, M. I. Ross, J. M. Kirkwood, M. B. Atkins, J. A. Thompson, D. G. Coit, D. Byrd, R. Desmond, Y. Zhang, P.-Y. Liu, G. H. Lyman, A. Morabito, Prognostic factors analysis of 17,600 melanoma patients: Validation of the American Joint Committee on Cancer melanoma staging system. J. Clin. Oncol. 19, 3622–3634 (2001).
- I. Satzger, B. Völker, A. Meier, A. Kapp, R. Gutzmer, Criteria in sentinel lymph nodes of melanoma patients that predict involvement of nonsentinel lymph nodes. *Ann. Surg. Oncol.* 15, 1723–1732 (2008).
- R. L. Morton, K. Howard, J. F. Thompson, The cost-effectiveness of sentinel node biopsy in patients with intermediate thickness primary cutaneous melanoma. *Ann. Surg. Oncol.* 16, 929–940 (2009).
- C. M. Balch, J. E. Gershenwald, S.-J. Soong, J. F. Thompson, M. B. Atkins, D. R. Byrd, A. C. Buzaid, A. J. Cochran, D. G. Coit, S. Ding, A. M. Eggermont, K. T. Flaherty, P. A. Gimotty, J. M. Kirkwood, K. M. McMasters, M. C. Mihm Jr., D. L. Morton, M. I. Ross, A. J. Sober, V. K. Sondak, Final version of 2009 AJCC melanoma staging and classification. *J. Clin. Oncol.* 27, 6199–6206 (2009).
- I. Stoffels, H. von der Stück, C. Boy, T. Pöppel, N. Körber, M. Weindorf, J. Dissemond, D. Schadendorf, J. Klode, Indocyanine green fluorescence-guided sentinel lymph node biopsy in dermatooncology. J. Dtsch. Dermatol. Ges. 10, 51–57 (2012).
- A. C. J. van Akkooi, M. G. Bouwhuis, J. H. W. de Wilt, M. Kliffen, P. I. M. Schmitz, A. M. M. Eggermont, Multivariable analysis comparing outcome after sentinel node biopsy or therapeutic lymph node dissection in patients with melanoma. *Br. J. Surg.* 94, 1293–1299 (2007).
- J. M. Thomas, Sentinel-lymph-node biopsy for cutaneous melanoma. N. Engl. J. Med. 365, 569–570 (2011).
- R. Riber-Hansen, N. Hastrup, O. Clemmensen, N. Behrendt, S. Klausen, M. Ramsing, E. Spaun, S. J. Hamilton-Dutoit, T. Steiniche, Treatment influencing down-staging in EORTC Melanoma Group sentinel node histological protocol compared with complete step-sectioning: A national multicentre study. *Eur. J. Cancer* 48, 347–352 (2012).
- 14. O. E. Nieweg, False-negative sentinel node biopsy. Ann. Surg. Oncol. 16, 2089–2091 (2009).
- D. L. Morton, J. F. Thompson, A. J. Cochran, N. Mozzillo, O. E. Nieweg, D. F. Roses, H. J. Hoekstra, C. P. Karakousis, C. A. Puleo, B. J. Coventry, M. Kashani-Sabet, B. M. Smithers, E. Paul, W. G. Kraybill, J. G. McKinnon, H.-J. Wang, R. Elashoff, M. B. Faries; MSLT Group, Final trial report of sentinel-node biopsy versus nodal observation in melanoma. N. Engl. J. Med. 370, 599–609 (2014)
- K. M. Tichauer, K. S. Samkoe, J. R. Gunn, S. C. Kanick, P. J. Hoopes, R. J. Barth, P. A. Kaufman, T. Hasan, B. W. Pogue, Microscopic lymph node tumor burden quantified by macroscopic dual-tracer molecular imaging. *Nat. Med.* 20, 1348–1353 (2014).
- L. V. Wang, L. Gao, Photoacoustic microscopy and computed tomography: From bench to bedside. Annu. Rev. Biomed. Eng. 16, 155–185 (2014).
- V. Ntziachristos, D. Razansky, Molecular imaging by means of multispectral optoacoustic tomography (MSOT). Chem. Rev. 110, 2783–2794 (2010).
- C. Kim, K. H. Song, F. Gao, L. V. Wang, Sentinel lymph nodes and lymphatic vessels: Noninvasive dual-modality in vivo mapping by using indocyanine green in rats—Volumetric spectroscopic photoacoustic imaging and planar fluorescence imaging. *Radiology* 255, 442–450 (2010).
- G. C. Langhout, D. J. Grootendorst, O. E. Nieweg, M. W. J. M. Wouters, J. A. van der Hage, J. Jose, H. van Boven, W. Steenbergen, S. Manohar, T. J. M. Ruers, Detection of melanoma metastases in resected human lymph nodes by noninvasive multispectral photoacoustic imaging. *Int. J. Biomed. Imaging* 2014, 163652 (2014).
- D. J. Grootendorst, J. Jose, M. W. Wouters, H. van Boven, J. Van der Hage, T. G. Van Leeuwen, W. Steenbergen, S. Manohar, T. J. M. Ruers, First experiences of photoacoustic imaging for detection of melanoma metastases in resected human lymph nodes. *Lasers Surg. Med.* 44, 541–549 (2012).
- G. Balasundaram, C. J. H. Ho, K. Li, W. H. Driessen, U. S. Dinish, C. L. Wong, V. Ntziachristos, B. Liu, M. Olivo, Molecular photoacoustic imaging of breast cancer using an actively targeted conjugated polymer. *Int. J. Nanomedicine* 10, 387–397 (2015).
- D. Razansky, N. J. Harlaar, J. L. Hillebrands, A. Taruttis, E. Herzog, C. J. Zeebregts, G. M. van Dam, V. Ntziachristos, Multispectral optoacoustic tomography of matrix metalloproteinase activity in vulnerable human carotid plaques. *Mol. Imaging Biol.* 14, 277–285 (2012).
- S. V. Hudson, J. S. Huang, W. Yin, S. Albeituni, J. Rush, A. Khanal, J. Yan, B. P. Ceresa, H. B. Frieboes, L. R. McNally, Targeted noninvasive imaging of EGFR-expressing orthotopic pancreatic cancer using multispectral optoacoustic tomography. Cancer Res. 74, 6271–6279 (2014).
- J.-T. Oh, M.-L. Li, H. F. Zhang, K. Maslov, G. Stoica, L. V. Wang, Three-dimensional imaging of skin melanoma in vivo by dual-wavelength photoacoustic microscopy. *J. Biomed. Opt.* 11, 034032 (2006).

- J. Stritzker, L. Kirscher, M. Scadeng, N. C. Deliolanis, S. Morscher, P. Symvoulidis, K. Schaefer, Q. Zhang, L. Buckel, M. Hess, U. Donat, W. G. Bradley, V. Ntziachristos, A. A. Szalay, Vaccinia virus-mediated melanin production allows MR and optoacoustic deep tissue imaging and laser-induced thermotherapy of cancer. *Proc. Natl. Acad. Sci. U.S.A.* 110, 3316–3320 (2013).
- D. McCormack, M. Al-Shaer, B. S. Goldschmidt, P. S. Dale, C. Henry, C. Papageorgio, K. Bhattacharyya, J. A. Viator, Photoacoustic detection of melanoma micrometastasis in sentinel lymph nodes. J. Biomech. Eng. 131, 074519 (2009).
- N. K. Tafreshi, X. Huang, V. E. Moberg, N. M. Barkey, V. K. Sondak, H. Tian, D. L. Morse, J. Vagner, Synthesis and characterization of a melanoma-targeted fluorescence imaging probe by conjugation of a melanocortin 1 receptor (MC1R) specific ligand. *Bioconjug. Chem.* 23, 2451–2459 (2012).
- I. Stoffels, J. Dissemond, T. Pöppel, D. Schadendorf, J. Klode, Intraoperative fluorescence imaging for sentinel lymph node detection: Prospective clinical trial to compare the usefulness of indocyanine green vs technetium Tc 99m for identification of sentinel lymph nodes. *JAMA Surg.* 150, 617–623 (2015).
- C. Voit, A. C. J. Van Akkooi, G. Schäfer-Hesterberg, A. Schoengen, K. Kowalczyk, J. C. Roewert, W. Sterry, A. M. M. Eggermont, Ultrasound morphology criteria predict metastatic disease of the sentinel nodes in patients with melanoma. J. Clin. Oncol. 28, 847–852 (2010).
- M. G. Cook, M. A. Green, B. Anderson, A. M. M. Eggermont, D. J. Ruiter, A. Spatz, M. W. Kissin, B. W. E. M. Powell; EORTC Melanoma Group, The development of optimal pathological assessment of sentinel lymph nodes for melanoma. *J. Pathol.* 200, 314–319 (2003).
- 32. A. C. van Akkooi, M. G. Cook, A. M. Eggermont, Increased sampling will lead to an increase in detection, but is it clinically relevant? Reply letter regarding: "Treatment influencing down-staging in EORTC Melanoma Group sentinel node histological protocol compared with complete step-sectioning: A national multicentre study" by Riber-Hansen et al. Eur. J. Cancer 48, 2488–2489 (2012).
- C. Mitteldorf, H. P. Bertsch, A. Zapf, C. Neumann, L. Kretschmer, Cutting a sentinel lymph node into slices is the optimal first step for examination of sentinel lymph nodes in melanoma patients. *Mod. Pathol.* 22, 1622–1627 (2009).
- I. Stoffels, M. Müller, M. H. Geisel, J. Leyh, T. Pöppel, D. Schadendorf, J. Klode, Cost-effectiveness
 of preoperative SPECT/CT combined with lymphoscintigraphy vs. lymphoscintigraphy for sentinel lymph node excision in patients with cutaneous malignant melanoma. *Eur. J. Nucl. Med. Mol. Imaging* 41, 1723–1731 (2014).
- W. L. Cheung, R. R. Patel, A. Leonard, B. Firoz, S. A. Meehan, Amelanotic melanoma: A detailed morphologic analysis with clinicopathologic correlation of 75 cases. *J. Cutan. Pathol.* 39, 33–39 (2012).
- A. E. Giuliano, A. J. Cochran, D. L. Morton, Melanoma from unknown primary site and amelanotic melanoma. Semin. Oncol. 9, 442–447 (1982).
- I. Stoffels, C. Boy, T. Pöppel, J. Kuhn, K. Klötgen, J. Dissemond, D. Schadendorf, J. Klode, Association between sentinel lymph node excision with or without preoperative SPECT/CT and metastatic node detection and disease-free survival in melanoma. *JAMA* 308, 1007–1014 (2012)
- C. Garbe, A. Hauschild, M. Volkenandt, D. Schadendorf, W. Stolz, U. Reinhold, R.-D. Kortmann, C. Kettelhack, B. Frerich, U. Keilholz, R. Dummer, G. Sebastian, W. Tilgen, G. Schuler, A. Mackensen, R. Kaufmann, Evidence-based and interdisciplinary consensus-based German guidelines: Systemic medical treatment of melanoma in the adjuvant and palliative setting. *Melanoma Res.* 18, 152–160 (2008).
- I. Stoffels, J. Dissemond, A. Körber, U. Hillen, T. Poeppel, D. Schadendorf, J. Klode, Reliability
 and cost-effectiveness of sentinel lymph node excision under local anaesthesia versus
 general anaesthesia for malignant melanoma: A retrospective analysis in 300 patients with

- malignant melanoma AJCC Stages I and II. J. Eur. Acad. Dermatol. Venereol. 25, 306–310 (2011)
- J. Klode, T. Poeppel, C. Boy, S. Mueller, D. Schadendorf, A. Körber, I. Stoffels, J. Dissemond, Advantages of preoperative hybrid SPECT/CT in detection of sentinel lymph nodes in cutaneous head and neck malignancies. *J. Eur. Acad. Dermatol. Venereol.* 25, 1213–1221 (2011).
- L. Barthelmes, A. Goyal, R. G. Newcombe, F. McNeill, R. E. Mansel; NEW START and ALMANAC study groups, Adverse reactions to patent blue V dye—The NEW START and ALMANAC experience. Eur. J. Surg. Oncol. 36, 399–403 (2010).
- M. Xu, L. V. Wang, Universal back-projection algorithm for photoacoustic computed tomography. Phys. Rev. E Stat. Nonlin. Soft Matter Phys. 71, 016706 (2005).
- S. Tzoumas, N. Deliolanis, S. Morscher, V. Ntziachristos, Unmixing molecular agents from absorbing tissue in multispectral optoacoustic tomography. *IEEE Trans. Med. Imaging* 33, 48–60 (2014).
- 44. V. G. Prieto, S. H. Clark, Processing of sentinel lymph nodes for detection of metastatic melanoma. *Ann. Diagn. Pathol.* **6**, 257–264 (2002).
- C. Garbe, A. Hauschild, M. Volkenandt, D. Schadendorf, W. Stolz, U. Reinhold, R.-D. Kortmann, C. Kettelhack, B. Frerich, U. Keilholz, R. Dummer, G. Sebastian, W. Tilgen, G. Schuler, A. Mackensen, R. Kaufmann, Evidence and interdisciplinary consense-based German guidelines: Diagnosis and surveillance of melanoma. *Melanoma Res.* 17, 393–399 (2007).
- J. A. Jensen, S. I. Nikolov, K. L. Gammelmark, M. H. Pedersen, Synthetic aperture ultrasound imaging. *Ultrasonics* 44 (Suppl. 1), e5–e15 (2006).

Acknowledgments: We thank E. Nasonova for her support with the MSOT/ultrasound prototype. Funding: This work was supported by a grant (An-2012-0036) from the Mercator Research Center Ruhr and by a grant (no. 2013.113.1) from the Wilhelm Sander-Stiftung. S.M., N.C.B., J.C., and T.C.P.S. were supported by a funding from the German Federal Ministry of Education and Research (BMBF) under the GO-Bio program (FKZ 0315978) as well as funding from European Union Seventh Framework Programme (FP7/2007-2013) under grant agreement no. 317744 (FAMOS). Author contributions: I.S. and J.K. designed the trial. I.S., S.M., N.C.B., and J.K. developed the methodology. I.S., J.L., T.C.P.S., J.C., N.C.B., K.G., and U.H. contributed to the recruitment of patients and tissues. I.S., S.M., I.H., T.D.P., N.C.B., D.S., A.R., M.G., and J.K. analyzed and interpreted the data, I.S., H.S.B., and J.K. performed statistical analysis. I.S., N.C.B., K.G., A.R., D.S., M.G., and J.K. wrote, edited, and approved the manuscript. M.G. and J.K. supervised the study. Competing interests: S.M., N.C.B, T.C.P.S., and J.C. are employees of iThera Medical. D.S. reported receiving consultancy fees, having board membership, and receiving lecture fees from GlaxoSmithKline, Novartis, Amgen, Bristol-Myers Squibb, Roche, Genentech, Boehringer Ingelheim, and MSD. M.G. reported receiving consultancy fees from Teva. The other authors declare no competing financial interests. Data and materials availability: Full patient data sets and corresponding imaging data are available upon request from the corresponding author.

Submitted 30 July 2015 Accepted 12 November 2015 Published 9 December 2015 10.1126/scitranslmed.aad1278

Citation: I. Stoffels, S. Morscher, I. Helfrich, U. Hillen, J. Lehy, N. C. Burton, T. C. P. Sardella, J. Claussen, T. D. Poeppel, H. S. Bachmann, A. Roesch, K. Griewank, D. Schadendorf, M. Gunzer, J. Klode, Metastatic status of sentinel lymph nodes in melanoma determined noninvasively with multispectral optoacoustic imaging. *Sci. Transl. Med.* 7, 317ra199 (2015).



Metastatic status of sentinel lymph nodes in melanoma determined noninvasively with multispectral optoacoustic imaging

Ingo Stoffels, Stefan Morscher, Iris Helfrich, Uwe Hillen, Julia Lehy, Neal C. Burton, Thomas C. P. Sardella, Jing Claussen, Thorsten D. Poeppel, Hagen S. Bachmann, Alexander Roesch, Klaus Griewank, Dirk Schadendorf, Matthias Gunzer and Joachim Klode (December 9, 2015)

Science Translational Medicine 7 (317), 317ra199. [doi: 10.1126/scitranslmed.aad1278]

Editor's Summary

Imaging melanoma metastasis

Avoiding invasive biopsy altogether, an imaging technique that relies on endogenous biomolecules to generate acoustic signals could be used to detect metastases in the body. Stoffels *et al.* devised a multispectral optoacoustic tomography (MSOT) approach that could image the pigment melanin in lymph nodes. Melanin would only be present in the lymph nodes if the primary cancer—melanoma—had spread to distant locations. The authors used handheld MSOT detectors and a near-infrared fluorophore (which pools in lymph nodes) to image metastases in patients, and complemented these optoacoustic images with ultrasound to gain a complete picture of each lymph node's status. Such a noninvasive approach could reduce the number of patients subjected to sentinel lymph node surgical excision by "ruling out" metastasis.

The following resources related to this article are available online at http://stm.sciencemag.org.

This information is current as of December 16, 2015.

Article Tools Visit the online version of this article to access the personalization and

article tools:

http://stm.sciencemag.org/content/7/317/317ra199

Supplemental "Supplementary Materials"

Materials http://stm.sciencemag.org/content/suppl/2015/12/07/7.317.317ra199.DC1

Related Content The editors suggest related resources on *Science*'s sites:

http://stm.sciencemag.org/content/scitransmed/4/134/134ps11.full http://stm.sciencemag.org/content/scitransmed/3/71/71ra15.full http://stm.sciencemag.org/content/scitransmed/7/310/310ra169.full http://stm.sciencemag.org/content/scitransmed/7/303/303ra138.full http://stm.sciencemag.org/content/scitransmed/4/116/116ra4.full http://stm.sciencemag.org/content/scitransmed/7/274/274ra19.full

Permissions Obtain information about reproducing this article:

http://www.sciencemag.org/about/permissions.dtl

Science Translational Medicine (print ISSN 1946-6234; online ISSN 1946-6242) is published weekly, except the last week in December, by the American Association for the Advancement of Science, 1200 New York Avenue, NW, Washington, DC 20005. Copyright 2015 by the American Association for the Advancement of Science; all rights reserved. The title Science Translational Medicine is a registered trademark of AAAS.